

Optimized field-stop collection for bright entangled photon pair sources

Alexander Lohrmann,¹ Aitor Villar,¹ Arian Stolk,¹ and Alexander Ling^{1,2}

¹*Centre for Quantum Technologies, National University of Singapore, 3 Science Drive 2, S117543*

²*Physics Department, National University of Singapore, 2 Science Drive 3, S117542*

(Dated: December 3, 2024)

We present an experimental demonstration of a bright and high fidelity polarization entangled photon pair source. The source is constructed using two critically phase matched β -Barium Borate crystals with parallel optical axes and photon pairs are collected after filtering with a circular field-stop. Near unity fidelities are obtained with detected pair rates exceeding 100 000 pairs/s/mW approaching the brightness of practical quasi-phase matched entangled photon sources. We find that the brightness scales linearly with the crystal length. We present models supporting the experimental data and propose strategies for further improvement. The source design is a promising candidate for emerging quantum applications outside of laboratory environments.

Entangled photon pairs lie at the heart of many emerging quantum technologies, such as quantum communication, key distribution and teleportation [1, 2]. An ongoing research problem is to develop sources of entangled photons that are bright and, at the same time, robust enough to be suitable for long term operation outside of laboratory environments. The main method of generating entangled photons is based on spontaneous parametric downconversion (SPDC) in nonlinear crystals.

One of the important considerations in the design of entangled photon sources is the effective collection angle of SPDC photons. This is critical because angle dependent phase effects can degrade the desired entangled state. Therefore, in many modern source designs[3–5] and applications[6, 7] single-mode fibers are commonly used to collect and spatially filter the entangled photon pairs. Single-mode fiber collection negates the angle dependent phase[8], but strongly reduces the source brightness. Collection through a field stop without further spatial filtering allows for a higher brightness, but requires knowledge of angle dependent phase effects[9–11].

Recently, we have demonstrated a new source design based on type-I, collinear, non-degenerate critical phase matching using two β -Barium Borate (BBO) crystals with parallel optical axes[12]. The parallel axes approach negates the effects of spatial walk-off which usually limits the collection brightness. This approach yielded photon pair rates of 65 000 pairs/s/mW when collected with a single-mode fiber, with a factor of 2.4 brighter than previous critically phase matched sources[3]. In this work, we further show that the spatial overlap of the emission modes leads to an almost perfect spatio-temporal compensation enabling the detection of maximally entangled photon pairs without single-mode filtering. We demonstrate pair rates of up to 100 000 pairs/s/mW with near-unity fidelity; furthermore, by relaxing the collection conditions, we achieve rates of 400 000 pairs/s/mW with QKD compatible fidelity.

The source design is sketched in Fig. 1(a). The pump with a vertical (extraordinary) polarization undergoes a walk-off within the first BBO crystal. Due to the type-I phase-matching, photon pairs with horizontal (ordinary)

polarization ($|H_s H_i\rangle_1$) are generated. An achromatic half-wave plate rotates the polarization of these photon pairs by 90° ($|H_s H_i\rangle_1 \rightarrow |V_s V_i\rangle_1$) while leaving the pump polarization unaffected. In the second crystal the pump again generates $|H_s H_i\rangle_2$ photons. The photon pair from the first crystal has extraordinary polarization in the second crystal and therefore also undergoes a walk-off in the same direction as the pump. This leads to an almost perfect spatial overlap of the SPDC emission modes from the two crystals. A small spatial mismatch between the two modes exists due to the different walk-off angles of pump and down-converted photons. For the purpose of the present work, this mismatch is negligible. We point out that this configuration enables the full pump power to be used in each crystal (in contrast to the conventional geometry using *crossed crystals*) yielding at least a twofold enhancement in the entangled pair rates[12].

One of the most important consequences that arises from the spatial overlap is the near-optimal spatio-temporal compensation. This can be understood when adding spatial considerations to the well-known temporal compensation scheme[3], which we will describe in the following. In general, the state generated after the two BBO crystals can be written as,

$$|\Phi\rangle = \frac{1}{\sqrt{2}} (|H_s H_i\rangle_2 + e^{i\Delta\varphi} |V_s V_i\rangle_1), \quad (1)$$

where $\Delta\varphi$ denotes the phase difference between the two emission processes. In order to generate one of the two maximally entangled Bell states, Φ^\pm , (here we assume Φ^- for convenience) in type-I phase-matching, the phase difference $\Delta\varphi$ must be constant in all spatial and spectral degrees of freedom. In practice, variation in the spatial degree of freedom can be negated by scrambling the spatial information using for example single-mode fiber collection. However, to enable collection without single-mode filtering, the spatial phase must be considered.

To determine the total phase difference, we sum the phase acquired by the individual photons as they pass through the elements of the experimental setup,

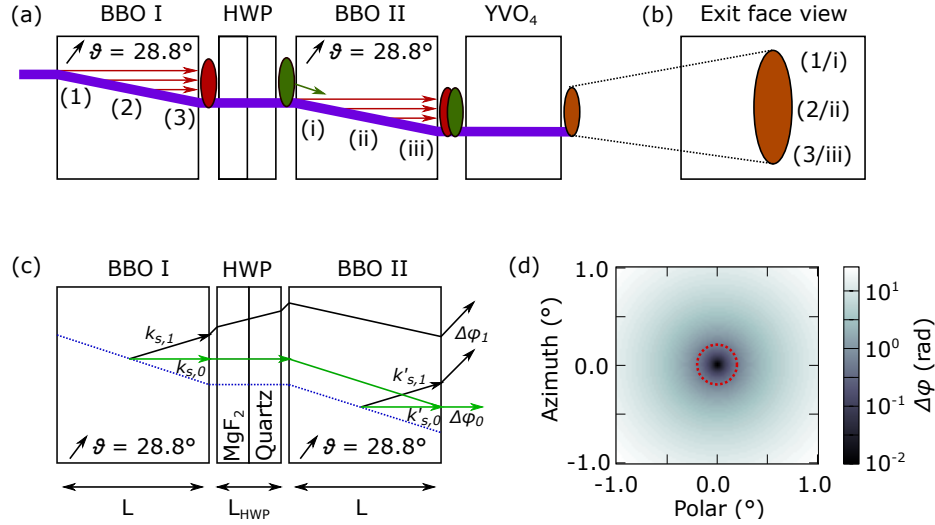


FIG. 1. (a) Basic principle of the parallel crystal configuration. The numbers 1-3 and i-iii indicate three possible SPDC generation positions for each crystal. The colors indicate the different photon polarizations (green: $|VV\rangle$, red: $|HH\rangle$). (b) Sketch of the SPDC spatial distribution at the exit face of the second crystal. The numbers 1-3 and i-iii indicate the photon origin as depicted in (a). (c) Signal (idler omitted for clarity) ray propagation diagram for collinear (green) and non-collinear emission (black). Pump indicated in blue. The angle dependence of the phase difference originates from the effective path length difference. (d) Phase-difference map as a function of the azimuthal and polar opening angles for the signal ray in air. The region inside the red circle indicates a region of approximately constant phase difference. (Color online)

$$\Delta\varphi(\lambda, \vec{x}, \vec{\alpha}) = \sum_i \varphi^H(\lambda, \vec{x}, \vec{\alpha}) - \sum_i \varphi^V(\lambda, \vec{x}, \vec{\alpha}), \quad (2)$$

where λ denotes the photon wavelength, \vec{x} the position of down-conversion and $\vec{\alpha}$ the signal emission angle. Any deviation from a constant value for $\Delta\varphi$ will lead to a mixed entangled state. In practice, the wavelength dependence of $\Delta\varphi$ is compensated with a birefringent temporal compensator [3, 12] (yttrium orthovanadate, YVO₄ in Fig. 1(a)). This leaves only spatial dependencies, $\Delta\varphi = \Delta\varphi(\vec{x}, \vec{\alpha})$.

In previous work with type-I SPDC using crossed crystals, phase-compensation is usually calculated for photon pairs generated in the center of each crystal. Photons are

collected only from a small effective interaction region and the rest of the emission is not only spatially distinguishable, but also deviates in the total phase difference. The detrimental impact of the non-constant phase difference can be overcome by using thin crystals or single-mode fiber collection.

In the present work, phase-compensation is achieved for each photon pair regardless of the downconversion location within the crystals. For example, photon pairs generated at the entry face of the first crystal are spatially indistinguishable from photon pairs born at the corresponding position in the second crystal (see Fig. 1(b)). This allows the collection of SPDC photons through a field stop without single-mode filtering. Note that this is a particular feature of the parallel crystal configuration. In the anti-parallel case, the phase difference is not constant over the emission profile and field-stop collection always leads to mixed entangled states.

Without single-mode filtering, angle dependent effects must be considered. An additional phase difference arises from the different path lengths when photon pairs are emitted under an angle (see Fig. 1(c)). The phase difference after the temporal compensator is shown in Fig. 1(d) as a function of polar and azimuthal opening angle. To collect the maximally entangled Bell state we need to restrict the SPDC emission angle appropriately. The angle dependent phase can in principle be compensated by additional birefringent crystals, where an opposite but equal angular effect is introduced.

The implementation of the entangled photon source is shown in Fig. 2. The output from a collimated, narrow-band 405 nm laser diode ($\Delta\nu \leq 160$ MHz) is used to gen-

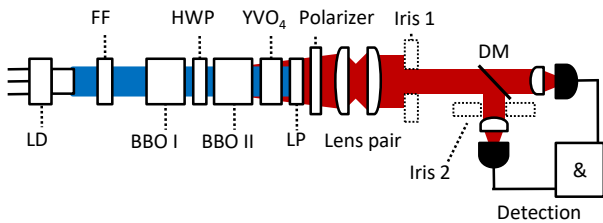


FIG. 2. Sketch of the experimental setup. LD: laser diode, FF: fluorescence filter, HWP: half-wave plate, LP: long-pass filter, DM: dichroic mirror. An Iris is used to control the opening angle of the SPDC light that reaches the detectors. It can be placed either before splitting signal and idler (Iris 1) or after the dichroic mirror in the signal arm (Iris 2). (Color online)

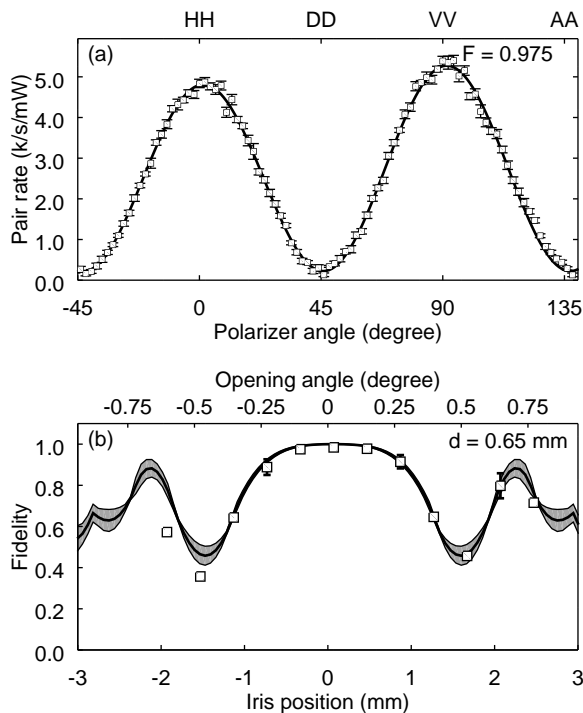


FIG. 3. (a) Detected photon pair rate when using a single polarizer acting simultaneously on signal and idler photons. In this case the iris was centered (iris position = 0 mm). The opening diameter of the iris was 0.65 mm. The visibility of the curve is 94%. (b) Fidelity with respect to vertical iris translation. The solid line shows Eq. 2, where $\bar{\alpha}$ is assumed to be linear in iris position. The spread indicates uncertainty interval due to iris diameter uncertainty (± 0.1 mm). Squares are experimental data. We observe a revival of fidelity with the ideal Bell state, showing the expected cyclic behavior of the phase.

erate SPDC in the 6 mm BBO crystals (optical axis angle $\theta = 28.8^\circ$) set for type-I, collinear phase matching. The photons are non-degenerate at 785 nm and 837 nm. The down-converted photons are collimated using a lens pair (full-width-at-half-maximum: 2.3 mm) and split according to their wavelengths and detected using Geiger-mode avalanche photo diodes (GM-APD).

To restrict the opening angles of signal and idler photons, a field stop can be placed in the collimated beam (Iris 1 in Fig. 2). This allows the fidelity and brightness of the source to be actively controlled by the field-stop diameter. Alternatively, the field stop can be placed in the signal or idler arm and scanned to access individual opening angles.

To characterize an unknown quantum state, full quantum state tomography is usually employed. However, with some reasonable assumptions regarding the generated state, the measurement can be greatly simplified. As the phasematching prevents the generation of $|HV\rangle$ and $|VH\rangle$ components, the generated state is mainly im-

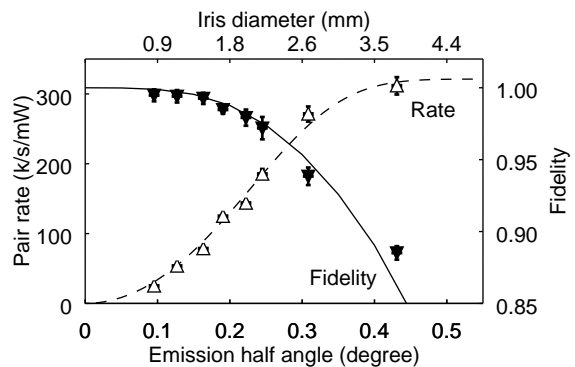


FIG. 4. Brightness (open triangles) and fidelity (filled triangles) as a function of emission angle for a source using 6 mm BBO crystals. The emission angle was calculated from the iris diameter. An error function was fitted to the brightness curve as the SPDC emission follows approximately a Gaussian angular distribution. The solid line describes the fidelity calculated from the phase difference (no free parameter).

pacted by three parameters, namely the imbalance between the polarization components, the purity of the generated Bell state and an incorrect phase.

The Bell state fidelity of the source can be estimated by partial quantum state tomography using a single polarizer after the temporal compensation crystal. This projects signal and idler in the same linear polarization basis and leads to a unique signature for the maximally entangled Bell states Φ^+ (zero contrast curve) and Φ^- (full contrast curve)[12].

We validated the angle dependent phase model by scanning the field stop in the signal arm and determined the fidelity at each position. The fidelity extracted when the field stop is in the center of the signal beam is $F = 0.975 \pm 0.003$ (see Fig. 3(a)). The fidelity when the field stop is translated across the signal beam in azimuthal direction is shown in Fig. 3(b). The model (grey shaded area) was derived from the phase difference map, where the opening angle was used as a fitting parameter. The model was also convolved with the field-stop diameter to account for the limited measurement resolution. The measurement indicates that diverging photon pairs with opening angles greater than 0.25° must be blocked to ensure a high state fidelity. The model is in agreement with the experimental results. In particular, the revival of the fidelity for large opening angles confirms the relationship between phase and emission opening angle. This result holds for both, polar and azimuthal directions.

In the final step, we placed the field stop in the collimated beam before splitting signal and idler photons and measured the brightness as a function of the emission angle by gradually opening the aperture. The brightness is measured at low pump power of $P \leq 100 \mu\text{W}$ to avoid saturating the passively quenched single photon detectors. The source brightness increased as expected for larger collection angles; with the opened aperture, we observed

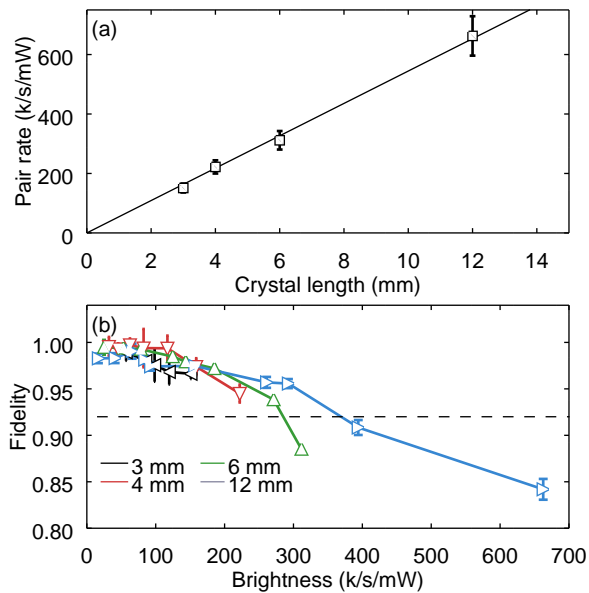


FIG. 5. (a) Brightness with fully opened iris (0.45° half angle) for various crystal lengths. The linear scaling indicates that pump and collection modes are in the thin crystal regime. (b) Correlation between fidelity and brightness for multiple crystal lengths. The brightness is controlled by the iris diameter. The dashed line indicates the QBER limit for the Ekert protocol of $\text{QBER} \leq 15\%$

a pair rate of 321 ± 11 k/s/mW (see Fig. 4). The observed pair to singles ratios are approximately constant over this range with $18.7 \pm 0.9\%$ and $20.0 \pm 0.9\%$ for signal and idler, respectively. Collection of higher pair rates is possible by increasing the effective numerical aperture of the system to collect photons at larger opening angles, at the expense of state fidelity.

We then measured the fidelity for different emission half angles and determined a clear degradation of the fidelity for emission half angles above 0.3° as predicted. For a collection angle below 0.1° the fidelity reached near unity values of $F = 0.995^{+0.005}_{-0.007}$. The trend is shown in Fig. 4 and can be well described by the model (black line). These results indicate that, by restricting the emission angle, a high Bell state fidelity of $F \approx 0.99$ can be achieved at detected pair rates of more than 100 000 pairs/s/mW without pump shaping or spectral filtering. This is particularly interesting for applications outside of laboratory environments, where critically phase matched sources are thought to be advantageous due to their relative temperature stability.

We repeated the experiment for various crystal lengths from 3 mm to 12 mm. The maximal brightness with the fully opened aperture is shown in Fig. 5(a). The brightness follows a linear trend with a pair rate of 54.5 ± 0.9 kpairs/s/mW/mm indicating that the collection conditions lie in the thin crystal regime[13].

The correlation between source brightness and fidelity is shown in Fig. 5(b) for different crystal lengths showing

that the increase in brightness occurs at the expense of fidelity. This imposes an upper limit for the brightness with acceptable fidelity. One future strategy to improve the fidelity at higher brightness is to perform phase compensation with a single birefringent lens. Such a lens could be used to simultaneously compensate any remaining spatial distinguishability caused by the different spatial origins of the $|HH\rangle$ and $|VV\rangle$ pairs.

In conclusion, we have demonstrated that type-I, collinear, critical phase-matching can be used to generate entangled photon pairs with rates that are comparable to those in quasi phase-matched sources. In the parallel crystal geometry, the beneficial spatio-temporal compensation enables the use of free-space detection which greatly enhances the rate of detected photon pairs. One essential feature of the source is that the pair rate can be controlled by restricting the SPDC emission angle. If high fidelity is needed, the pair rate may be reduced to ensure a near unity fidelity, while for non-critical applications pair rates of more than 0.4 million pairs per second are possible.

In the future, an additional birefringent crystal may be added to the source to compensate the spatial mismatch between the $|HH\rangle_2$ and $|VV\rangle_1$ pairs. In addition, the angle dependence of the phase difference may be compensated by an additional birefringent lens. The small footprint, its robustness and the ease of alignment make this source an ideal candidate for applications involving free-space transmission.

METHODS

The analysis of the single polarizer measurement is described in [12]. With the assumption that no $|HV\rangle$ and $|VH\rangle$ components are generated in the source, the generated state simplifies to a two-level system comprising $|HH\rangle$ and $|VV\rangle$ states,

$$\rho = p \left(\sqrt{x} |HH\rangle + e^{i\theta} \sqrt{1-x} |VV\rangle \right) \left(\sqrt{x} \langle HH| + e^{-i\theta} \sqrt{1-x} \langle VV| \right) + \frac{(1-p)}{2} \left(|HH\rangle \langle HH| + |VV\rangle \langle VV| \right), \quad (3)$$

where p denotes the purity, x the balancedness of the Bell state and θ the relative phase. We project this state to the single polarizer measurement and fit the result to the experimental data to extract the parameters describing the simplified quantum state. From the simplified density matrix we can calculate the fidelity.

The single polarizer measurement on its own can not distinguish a mixed state from a rotated pure state. However, in the case of the measurement of translating a small iris (see Fig. 3), we know that the mixing is limited due to the selected small numerical aperture. The recovery

in fidelity beyond 0.5° supports this claim. This allows us to extract the phase information from our fit. When measuring the performance of the source at different iris sizes (see Fig. 4), the phase-compensation is adjusted for every data-point, and the phase mismatch with the desired state is assumed to be small compared to the mixing. The decay in fidelity can thus be attributed to the state being unbalanced and/or mixed.

ACKNOWLEDGEMENTS

This program is supported by the National Research Foundation, Prime Ministers Office of Singapore, and the Ministry of Education, Singapore.

-
- [1] N. Gisin and R. Thew, *Nature photonics* **1**, 165 (2007).
 - [2] R. Horodecki, P. Horodecki, M. Horodecki, and K. Horodecki, *Reviews of modern physics* **81**, 865 (2009).
 - [3] P. Trojek and H. Weinfurter, *Applied Physics Letters* **92**, 211103 (2008).
 - [4] F. Steinlechner, P. Trojek, M. Jofre, H. Weier, D. Perez, T. Jennewein, R. Ursin, J. Rarity, M. W. Mitchell, J. P. Torres, *et al.*, *Optics express* **20**, 9640 (2012).
 - [5] F. Steinlechner, S. Ramelow, M. Jofre, M. Gilaberte, T. Jennewein, J. P. Torres, M. W. Mitchell, and V. Pruneri, *Optics express* **21**, 11943 (2013).
 - [6] J. Yin, Y. Cao, Y.-H. Li, S.-K. Liao, L. Zhang, J.-G. Ren, W.-Q. Cai, W.-Y. Liu, B. Li, H. Dai, *et al.*, *Science* **356**, 1140 (2017).
 - [7] F. Steinlechner, S. Ecker, M. Fink, B. Liu, J. Bavaresco, M. Huber, T. Scheidl, and R. Ursin, *Nature communi-*
cations **8**, 15971 (2017).
 - [8] S. F. Hegazy, Y. A. Badr, and S. S. Obayya, *Optical Engineering* **56**, 026114 (2017).
 - [9] P. G. Kwiat, E. Waks, A. G. White, I. Appelbaum, and P. H. Eberhard, *Physical Review A* **60**, R773 (1999).
 - [10] T. Kim, M. Fiorentino, and F. N. Wong, *Physical Review A* **73**, 012316 (2006).
 - [11] J. B. Altepeter, E. R. Jeffrey, and P. G. Kwiat, *Optics Express* **13**, 8951 (2005).
 - [12] A. Villar, A. Lohrmann, and A. Ling, *Optics Express* **26**, 12396 (2018).
 - [13] A. Ling, A. Lamas-Linares, and C. Kurtsiefer, *Physical Review A* **77**, 043834 (2008).